Estimating the Cross-Correlation Properties of Large-Scale Parameters in Multilink Distributed Antenna Systems

Synchronous Measurements Versus Repeated Measurements

Dahman, Ghassan; Flordelis, Jose; Tufvesson, Fredrik

Published in:
IEEE Transactions on Vehicular Technology

DOI:
10.1109/TVT.2017.2691474

2017

Document Version:
Peer reviewed version (aka post-print)

Estimating the Cross-Correlation Properties of Large-Scale Parameters in Multi-Link Distributed Antenna Systems: Synchronous Measurements versus Repeated Measurements

Ghassan Dahman, *Member, IEEE*, Jose Flordelis, *Student Member, IEEE*, and Fredrik Tufvesson, *Fellow, IEEE*

***Abstract*—It is essential to capture the cross-correlation properties of large-scale parameters (LSPs) among different base station links in cooperative multi-link systems in order to make realistic performance assessments. In this work, propagation measurements are used to study the cross-correlation properties of different LSPs, namely, large-scale fading, delay spread, azimuth spread, and elevation spread of four links. The inter-link cross-correlation coefficients of these LSPs are assessed based on two different measurement approaches: 1) synchronous measurements, where the values of the LSPs of the considered links are estimated from the same measurement run, and 2) repeated measurements, where the values of the LSPs of the considered links are estimated from different measurement runs. Repeated measurements are attractive because they are simpler and less expensive. In this paper, we address the following question: can repeated measurements be used instead of synchronous measurements in order to estimate the LSPs' cross-correlation properties of different links? Based on analysis of wideband synchronous and repeated multi-link measurements in a suburban microcell environment at 2.6 GHz, we found that: 1) the mean values of the cross-correlation coefficients are preserved with repeated measurements, and 2) the estimates of the cross-correlation coefficients from repeated measurements are less spread around the mean value than those from synchronous measurements. These findings are explained based on detailed investigation of specific measured cases and further supported by results obtained from Monte Carlo simulations.**

***Index Terms*—distributed antenna systems; multi-link systems; large-scale parameters; inter-link cross-correlation.**

I. Introduction

DUE to the increasing importance of multi-link communications and its applications in the next generation wireless systems, significant research effort is focusing on modeling the joint characteristics of multiple base station (BS) links. Providing such models is crucial in order to design/evaluate communication systems that employ multiple links and exploit the spatial distribution of the communication nodes, for example, Cooperative Multi-Point (CoMP) systems. It is always desirable to provide an accurate model to characterize the joint statistics of propagation parameters of different links based on measurements. In ideal cases, measurements should be carried out synchronously for different links despite the fact that the transmitting/receiving nodes might be physically separated. Overcoming this challenge in indoor scenarios can be achieved by connecting the distributed nodes by means of long RF cables [1], [2]. However, in outdoor scenarios, using RF cables is not an option because of the longer distances and the relatively high attenuation (several tens to couple of hundreds dB/km around 2 GHz carrier frequencies when low-loss RF cables are used).

In the literature, different systems allowing for performing multi-link synchronous measurements are reported: using dual synchronized channel sounders [3], [4], connecting the different transmitting nodes by means of fiber optics [5], [6], [7], [8], time stamping of individual snapshots [9], [10], [11], and transmitting frequency orthogonal sounding signals [12], [13]. Despite the valuable information available about the cross-correlation properties of multi-link channels, additional measurement campaigns are required in order to characterize more scenarios, e.g., more propagation environments and different antenna arrangements.

Due to their relative low complexity and cost, repeated measurements (i.e., performing the propagation measurements for one link at a time) are a very attractive option as long as they provide the same information as the synchronous ones. In [14], the authors studied the differences between two large-scale parameter (LSP) sets estimated for a *single* link (each LSP set was estimated from a separate measurement run) in order to evaluate the stationarity of the outdoor environment between repeated measurements. By analyzing the two repeated runs that were performed on the same track, the authors evaluated the similarity/difference between the time series of each LSP estimated from the two runs. The term de-correlation level was used to express the difference between maximal (100%) and the observed cross-correlation between the two time series. They found that a repeated (i.e., multi-run) measurement procedure causes less than 9% de-correlation of estimated delay and azimuth spreads. The authors concluded that large-scale characterization of multi-link systems can be performed sequentially with a single sounder. However, no explicit attempt based on actual synchronous multi-link measurements has been done in order to compare the similarity/difference between synchronous and repeated measurements in characterizing the cross-correlation properties of different, possibly distributed, links.

In this paper, we address the following question: can re-

This work has been supported by a grant from the Swedish Foundation for Strategic Research, SSF.

Ghassan Dahman, during this work, was with the Department of Electrical and Information Technology, Lund University, Lund, Sweden. He is now with the NSERC-Ultra Electronics TCS Industrial Chair, École de Technologie Suprieure (ÉTS), Montreal, Canada (email:ghassan.dahman@lacime.etsmtl.ca).

Jose Flordelis and Fredrik Tufvesson are with the Department of Electrical and Information Technology, Lund University, Lund, Sweden (email: {jose.flordelis, fredrik.tufvesson}@eit.lth.se).

peated measurements be used instead of synchronous measurements in order to estimate the cross-correlation properties of the LSPs for different links? We tackle this question by performing synchronous multi-link propagation measurements. These synchronous measurements were repeated three times using a predefined route in order to emulate repeated measurements. Then, the measurement data were used to compare the differences between synchronous measurements and repeated measurements in terms of estimating the cross-correlation properties of four LSPs - namely, the large-scale fading (LSF), the delay spread, the azimuth spread, and the elevation spread - of the different links. The rest of this paper is organized as follows. Sections II, and III include the description of the propagation measurement setup, and the data analysis procedure, respectively. The results and the conclusion are detailed in Sections IV, and V, respectively.

II. Measurements

A. Measurement Scenario and Equipment

The measurement campaign was carried out using the RUSK-LUND channel sounder [15] at 2.6 GHz with a measurement bandwidth of 40 MHz. The measurements took place at the campus of the Faculty of Engineering, LTH, Lund University, Lund, Sweden, in an area which can be best characterized as a sub-urban micro-cellular environment. The chosen setup consists of four transmit BSs, each of which is equipped with a single vertically polarized antenna element. The sounding signal is conveyed to each of the remote BS location through the optical backbone network of the campus by means of radio-over-fiber (RoF) transceivers.

The signal broadcasted by the BSs is received by a single mobile station (MS) equipped with 64 dual-polarized antenna elements in a stacked uniform cylindrical array configuration. The 512 (4 BSs $\times$ 128 MS antenna elements) transmit-receive channels are sounded in a time-multiplexed fashion, all of the receive antenna elements being visited in succession prior to switching to the next transmit antenna element. The data resulting from this operation is referred to as a *snapshot*. The sounder was wheel triggered at one snapshot per wavelength (one snapshot each, approximately, 11 cm). Please refer to [8] for more details about the equipment used.

B. BSs' Antenna Positions

The transmit antennas (one vertically polarized antenna element at each one of the four BSs) were placed outside the windows at the second and third floors of four different buildings, as shown in Fig. 1, which corresponds to 5 to 12 m above the ground level and 10 to 20 m below the surrounding buildings. The distances among the different BSs are between 60 to 200 m.

C. MS Travel Route

The MS was moving in a predefined route with a total length of 40.85 m (350 wavelengths), at a very low walking speed ($<$ 0.5 m/s). The measurements on this route were performed three times, each of which is called a *measurement run*. In each measurement run, the Single-Input Multiple-Output (SIMO) channels of the four links are recorded synchronously. In order to guarantee that the MS travels over the same trajectory when each measurement run is recorded, paint was used to mark the MS track.

Fig. 1. Aerial photo of the measurement area. Base station locations are indicated by labels BS-E, BS-S, BS-F and BS-M. The measurement route is plotted in blue color.

D. Channels' Propagation Conditions

The area in the middle of the four BSs is an open area with a small lake surrounded by high trees. The propagation conditions between the MS and three of the BSs transmit antennas can be described as obstructed line-of-sight, or non-line-of-sight. The propagation condition between the MS and the fourth BS is line-of-sight, though. The BSs are named BS-E, BS-S, BS-F and BS-M; and their corresponding links with the MS are named E, S, F, and M, respectively. Fig. 1 shows an aerial photo of the measurement area, where the positions of the BSs, and the MS travel route are marked.

For the considered propagation conditions, the quasi-WSSUS (Wide-Sense Stationary Uncorrelated Scattering) model holds, where the channel can be divided into small regions such that within each region the LSPs change slowly over time and frequency in comparison to the coherence time and the coherence frequency, respectively. Also, it should be emphasized that the reported results are based on considering a semi-static environment i.e., the large interacting objects are strictly stationary and there is no significant movement of any interacting object except sudden small movements of tree branches due to wind.

III. Data Analysis

A. Preprocessing

The raw data obtained from the measurements consists of the transfer functions of the SIMO channels of the different links, which are used to get their corresponding impulse response estimates (IREs). To mitigate the effect of noise from channel IREs, the approach of [16] is followed, where multipath echoes are declared valid in a specific delay bin with a probability of false-alarm of one per 5000 snapshots per link. Also, the IREs are subjected to a delay-gating filter, which was implemented by using a 700 m delay-window. This filter

This is the author's version of an article that has been published in this journal. Changes were made to this version by the publisher prior to publication.
The final version of record is available at http://dx.doi.org/10.1109/TVT.2017.2691474

eliminates all multipath components that are 700 m in excess of the Tx-Rx separation. Then, Space-Alternating Generalized Expectation-Maximization (SAGE) [17], [18], was applied to each IRE in order to extract the angle-of-arrival (in both azimuth and elevation), complex amplitude, and delay of each multipath component. Power compensation is applied to each of the remote transmit antenna elements in order to compensate for differences in gain due to amplifiers, optical transceivers and fibers. This power compensation step was based on, after deployment, measuring the transmitted power at the output of each amplifier (i.e., at the input of each BS antenna) during the calibration stage and then compensating the IREs for the power differences among the links. The extracted multipath components are then used to estimate instances of the LSPs as explained in the sequel.

B. Estimating the Large-Scale Parameters

The first step on estimating the LSPs is to decide on a proper number of snapshots over which time averaging is applied in order to eliminate the effect of the small-scale fading (SSF).

Let's start by using only a single snapshot, i.e., estimating the instantaneous parameters. In this case, the SAGE results of each single snapshot are used to calculate the instantaneous delay, azimuth, and elevation power profiles. Then, the instantaneous delay spread (σ_τ), azimuth spread (σ_ϕ), and elevation spread (σ_θ) are calculated as the normalized second-order central moments of their corresponding instantaneous power spectrum [19, pp. 113, 122].

LSF is defined as the power fluctuation over a large area where the small scale fading is averaged out. To extract the instantaneous LSF, the following steps were followed. The values of the instantaneous received power obtained for all snapshots and for all links are plotted against the distance from the MS to the BSs in double logarithmic scale, and a linear regression is performed according to

$$P_r(d)_{dB} = P_r(d_0)_{dB} - n10log_{10}(d/d_0) \tag{1}$$

where, $P_r(d)_{dB}$ is the received power at BS-MS distance, d, and $P_r(d_0)_{dB}$ is the received power at the reference distance, d_0.

It was found that the power decay exponent that minimizes the distance between the data samples and the line of (1) in the minimum mean square error (MMSE) sense is $n = 3.89$. Since this decay exponent is by definition related to the propagation environment, it was adopted as the slope of the lines that represent the best fit for each individual link. However, due to the height difference among the different BS, a different offset was calculated for each link in order to find the best fit for each link. Finally, the instantaneous LSF is estimated as the difference between the instantaneous received power and (1).

The instantaneous parameters of the three measurement runs were plotted against the MS travel distance for further investigations. It was found that, despite the fact that all plots of the three measurement runs have the same "trend", abrupt changes at certain locations exist which we attribute to the remaining SSF. In our case, the delay spread is found to be the LSP that experiences the highest abrupt changes (depicted in Fig. 2).

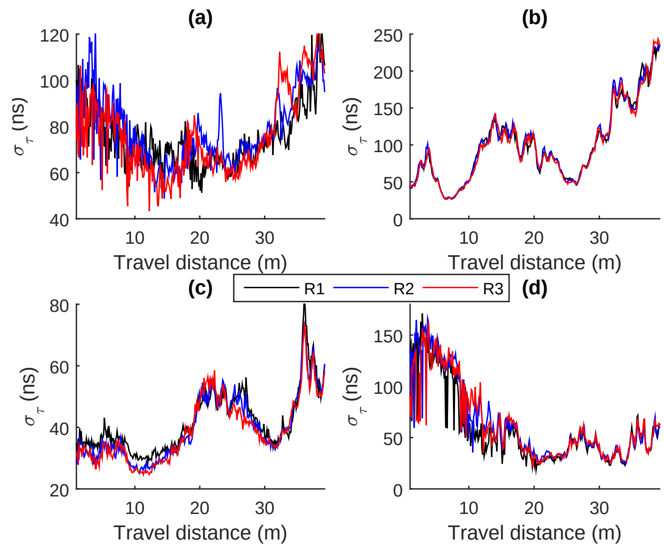

Fig. 2. The instantaneous delay spread estimates extracted for the three repeated measurements: (a) the E link, (b) the S link, (c) the F link, and (d) the M link. R1, R2, and R3 denote the first, second, and third measurement runs, respectively.

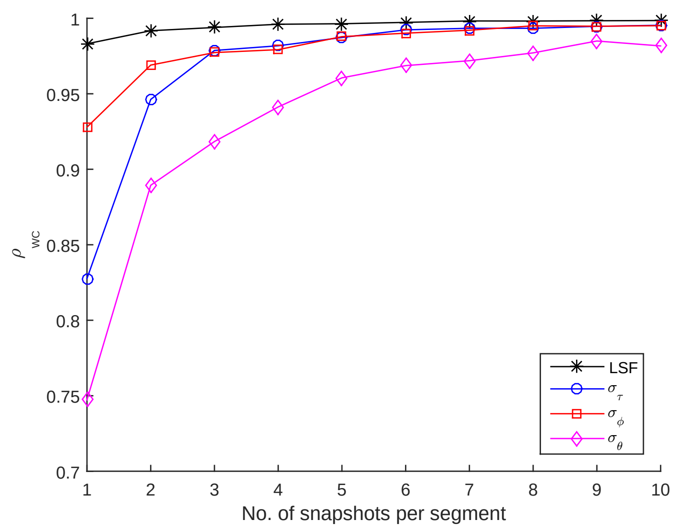

Fig. 3. Cross-correlation coefficients of the worst mismatch case as a function of the number of snapshots per segment

After having estimated the instantaneous parameters of each link, we now turn to estimating the average LSPs (i.e., time averaged over more than one snapshot). In order to do so, the measurement route is divided into S consecutive and disjoint segments, each with L snapshots. Then, for each segment and for each link, the LSF, delay spread (σ_τ), azimuth spread (σ_ϕ), and elevation spread (σ_θ) are calculated based on the SAGE results. It should be mentioned that, for all considered values of L over which time averaging is applied, the optimum decay exponent value ($n = 3.89$) stays unchanged.

C. Estimating the Averaging Segment Length

In order to find the value of the minimum segment length (L) that is enough to average out the effect of the SSF, we use the following arguments. Given that a distance of one wavelength is enough for the SSF to affect the channel parameters estimates as demonstrated in Fig. 2, and given that,

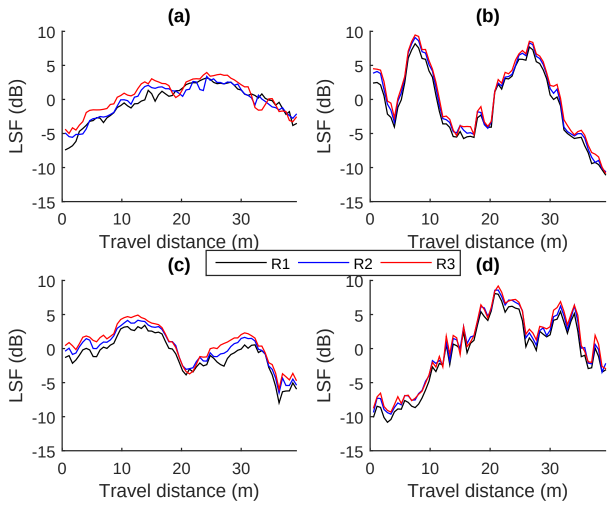

Fig. 4. The LSF estimates for the four links: (a) the E link, (b) the S link, (c) the F link, and (d) the M link. R1, R2, and R3 denote the first, second, and third measurement runs, respectively.

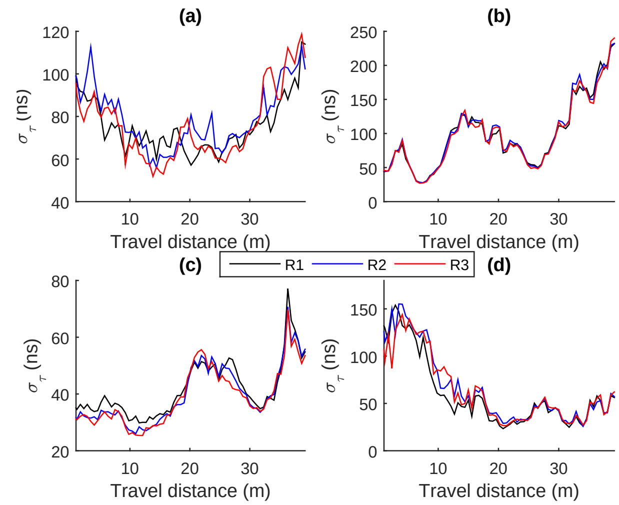

Fig. 5. The rms delay spread estimates for the four links: (a) the E link, (b) the S link, (c) the F link, and (d) the M link. R1, R2, and R3 denote the first, second, and third measurement runs, respectively.

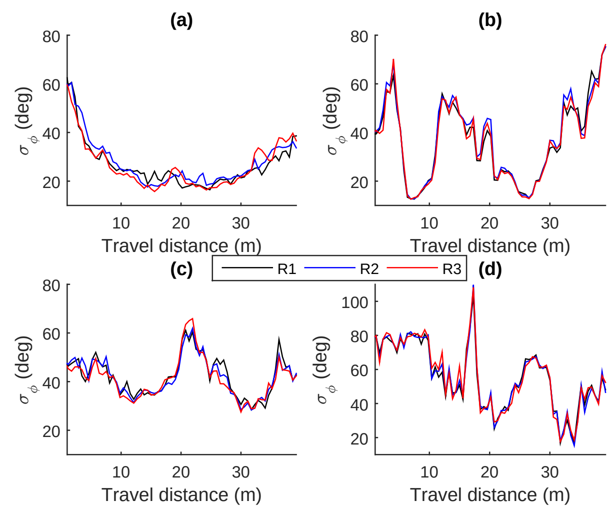

Fig. 6. The rms azimuth spread estimates for the four links: (a) the E link, (b) the S link, (c) the F link, and (d) the M link. R1, R2, and R3 denote the first, second, and third measurement runs, respectively.

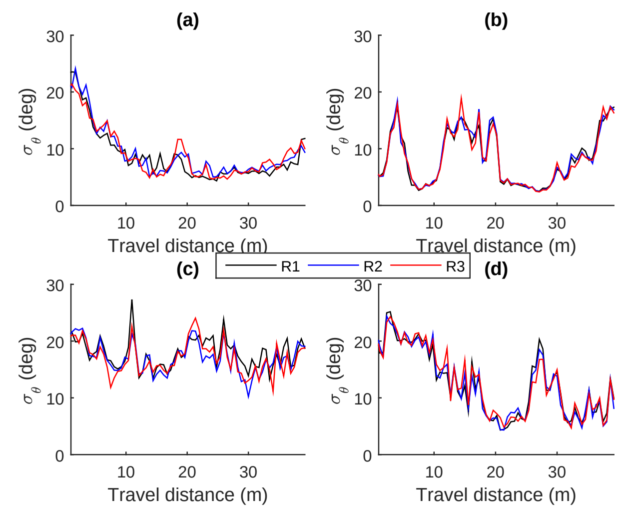

Fig. 7. The rms elevation spread estimates for the four links: (a) the E link, (b) the S link, (c) the F link, and (d) the M link. R1, R2, and R3 denote the first, second, and third measurement runs, respectively.

by definition, a wavelength distance does not affect the LSPs of the channel, we aim to find the minimum value of L that will keep each time series of the extracted LSPs, for all single links, almost perfectly correlated with another version of itself that is generated by misaligning the original received snapshots by an offset of one snapshot. Therefore, the following procedure is applied:

1) The number of snapshots per segment (i.e., L) is varied from 1 (i.e., instantaneous parameters), to a maximum of 10 snapshots. This upper limit of L (10 snapshots = 1.15 m) is an environment-dependent parameter and it is meant to be much smaller than the size of the main interacting objects in the measurement environment so that, after time-averaging is applied, their shadowing effect is preserved.
2) For each measurement run and for each link, the measured snapshots are used to generate two sequences of segments: a) an original sequence, where all the snapshots starting from snapshot no. 1 are included. In this case, the sth segment includes the snapshots from $(s-1)\times L+1$ to $s \times L$, where, $s = 1, 2, ..., S$, and b) a misaligned sequence, where the snapshots starting from snapshot no. 2 are included. In this case, the sth segment contains the snapshots from $(s-1)\times L+2$ to $s\times L+1$.
3) These two sequences of segments are used to estimate the LSPs. The output of this step is to generate two types of time series of LSPs: original LSP time series, and misaligned LSP time series.
4) The similarity between each two original and misaligned LSP time series (given that both of them are estimates of the same LSP of the same link in the same measurement run) is expressed by calculating the cross-correlation coefficient between them.
5) For each value of L, and for each one of the LSPs, the cross-correlation coefficient is calculated for each measurement run and for each link (3 runs $\times$ 4 links = 12 coefficients). Then the smallest value among these 12

coefficients is selected, which represents the **w**orst **c**ase cross-correlation coefficient (ρ_{WC}). Then, the values of ρ_{WC} are plotted against L in Fig. 3.

6) From Fig. 3, it is found that selecting $L = 5$ is enough to average out the SSF and to keep high cross-correlation values (greater than 0.96) between the original and misaligned time series of all considered LSPs.

As a result of the abovementioned steps, it was decided to time average over 5 snapshots (i.e., using 5 snapshot-long segments, which equals to about 58 cm) in order to extract the LSPs. For each segment, the LSF, delay spread (σ_τ), azimuth spread (σ_ϕ), and elevation spread (σ_θ) are estimated. Figs. 4-7 illustrate the extracted LSPs for the different measurement runs and for the different links.

D. Evaluating the Effect of Snapshot Alignment Error Among the Repeated Measurement Runs

As mentioned earlier, the repeated measurements were done carefully to guarantee minimum misalignment among the different runs. We believe that we had a maximum misalignment of half a wavelength among the different measurement runs. This estimation came from comparing the paint marks used to determine the starting and ending points of the MS trajectory at each measurement run. Theretofore, we conclude that the error in estimating the cross-correlation coefficients of the LSPs for the different link pairs due to snapshot alignment error (maximum of half a wavelength misalignment) is upper bounded by the error values associated with ρ_{WC} (where the worst case cross-correlation is analysis based on assuming an alignment error of one wavelength) as detailed in section III-C.

IV. RESULTS

A. Analysis Based on Measurement Data

The goal of this work is to study the differences, if any, in estimating the cross-correlation properties of the LSPs among different links using two types of measurements: synchronous and repeated measurements.

The cross-correlation coefficient of two time series X and Y is calculated as:

$$\rho_{X,Y} = E[(\frac{X-\mu_X}{\sigma_X})(\frac{Y-\mu_Y}{\sigma_Y})] \qquad (2)$$

where, μ_X and μ_Y are the means of X and Y, respectively. σ_X and σ_Y are the standard deviations of X and Y, respectively. $E(.)$ denotes the expectation operator. $\frac{X-\mu_X}{\sigma_X}$ and $\frac{Y-\mu_Y}{\sigma_Y}$ are the zero-mean unit-variance time series corresponding to X and Y, respectively, which will be utilized later when we closely inspect the time series of some of the estimated LSPs. Also, let's define C as the time series resulting from the element-wise multiplication of the two corresponding zero-mean unit-variance time series i.e., $C = (\frac{X-\mu_X}{\sigma_X}) \odot (\frac{Y-\mu_Y}{\sigma_Y})$, where $\odot$ denotes element-wise multiplication. The properties of C when the corresponding time series are estimated from synchronous measurements versus repeated measurements are also examined later.

1) Using the Measurement Data to Emulate Synchronous and Repeated Measurement Setups

As explained earlier, the synchronous measurements were repeated three times using a predefined route in order to emulate repeated measurements. Based on that, four LSPs are studied. In the measurement setup, we have four BS links denoted as: E, S, F, and M, resulting in 6 link pairs: ES, EF, EM, SF, SM, and FM. Hence, the cross-correlation properties of 24 cases (4 LSPs $\times$ 6 link pairs) are estimated. Given that we have performed 3 measurement runs, each of these 24 cross-correlations is estimated 6 times: 3 estimates using the synchronous measurement approach, and 3 estimates using the repeated measurement approach. For example: $\rho_{LSF,EF,Sync,R1}$ denotes the cross-correlation coefficient of the LSF between the E and the F links estimated from run 1 of the synchronous measurements. Similarly, $\rho_{LSF,EF,Rep,R1\&R2}$ denotes the cross-correlation coefficient of the LSF between the E and the F links estimated from the repeated measurements, where the LSF instances of the E link are estimated from run 1 and the LSF instances of the F link are estimated from run 2.

For each measurement approach (synchronous or repeated) and for each link pair, the 3 estimates of the cross-correlation coefficient of each LSP are characterized by their mean and standard deviation. Please notice that, when studying the repeated measurements, for each LSP, for each link pair, we get 6 estimates for each cross-correlation coefficient (given that, for example, $\rho_{LSF,EF,Rep,R1\&R2} \neq \rho_{LSF,EF,Rep,R2\&R1}$). However, we can only get 3 estimates when using the synchronous measurement approach. In order to guarantee fairness when comparing the means and the standard deviations of the cross-correlation estimates resulting from the synchronous versus the repeated measurement approaches, only 3 (out of the 6 possible) estimates of the repeated measurements are included. Table I lists the measurement runs that are used to get the cross-correlation estimates for the two approaches.

2) Calculating the Means, μ_{Sync} & μ_{Rep}, and the Standard Deviations, σ_{Sync} & σ_{Rep}, of the Cross-Correlation Estimates for the Synchronous and Repeated Measurements

Each cross-correlation coefficient estimate resulting from (2) is calculated based on two time series each with 70 LSP estimates, where the measurement run is divided into 70 5-wavelength non-overlapping segments. Based on Table I, three cross-correlation coefficient estimates (ρ_k), where $k = 1, 2, 3$ are calculated from the synchronous/repeated measurement runs. Then σ_{Sync} and σ_{Rep} are calculated as the standard deviations of their corresponding estimates, ρ_k. The values of μ_{Sync} and μ_{Rep} could be calculated using the same approach i.e., as the means of their corresponding estimates, ρ_k. However, in order to be able to: 1) test the statistical significance of each calculated value of μ_{Sync} (μ_{Rep}), and 2) test if two values (μ_{Sync} vs. μ_{Rep}) are significantly different or not, the Fisher's transformation [20, pp. 509-510], [21, pp. 274-277] is utilized in the evaluation of μ_{Sync} and μ_{Rep} as follows .

- The Fisher's transformation is used to transform each of the cross-correlation coefficient estimates (ρ_k) to a Fisher's z value, $z_k = tanh^{-1}(\rho_k)$. The resulting z is normally distributed with standard deviation $1/\sqrt{N-3}$, where $N = 70$ is the number of the non-overlapping segments.

- The average z values for the synchronous (repeated) measurements, Z_{Sync} (Z_{Rep}) are calculated based on averaging their corresponding z_k values. Then, $\mu_{_{Sync}}$ and $\mu_{_{Rep}}$ are calculated by applying the inverse Fisher's transform, i.e., $\mu_{_{Sync}} = tanh(Z_{Sync})$, and $\mu_{_{Rep}} = tanh(Z_{Rep})$ [22] [1].

The standard error (SE) in estimating Z_{Sync} and Z_{Rep} is $SE = 1/\sqrt{K(N-3)}$, where $K = 3$ is the number of estimates. The value of SE is found to be 0.07. Consequently:

- The Z_{Sync} and Z_{Rep} values that are not significantly different than zero (at significance level $\alpha = 5\%$) are disregarded from any further analysis and their corresponding $\mu_{_{Sync}}$, $\mu_{_{Rep}}$, $\sigma_{_{Sync}}$, and $\sigma_{_{Rep}}$ values are crossed-out in Tables II and III.
- The 95% confidence interval (CI) of the $\mu_{_{Sync}}$ and $\mu_{_{Rep}}$ estimates are reported in Table II.

3) *Comparing the Means and the Standard Deviations of the Cross-Correlation Estimates for Synchronous and Repeated Measurements*

By inspecting the values of the means ($\mu_{_{Sync}}$ vs. $\mu_{_{Rep}}$) and the standard deviations ($\sigma_{_{Sync}}$ vs. $\sigma_{_{Rep}}$) of the cross-correlation estimates in Tables II and III, it is found that:

- The means of the synchronous measurements and the repeated measurements are very similar, e.g., the difference $|\mu_{Sync} - \mu_{Rep}|/|\mu_{Sync}|$ exceeds 25% only in 6 cases (gray cells in Table II). This similarity is confirmed also by evaluating whether the Fisher's transformed means (Z_{Sync} and Z_{Rep}) are significantly different from one another or not (at significance level $\alpha = 5\%$). In all remaining cases (i.e., all cells which are not highlighted nor crossed-out in Table II), it is found that the null hypothesis - that the two correlations are not significantly different - can not be rejected.
- The standard deviations that are associated with the synchronous measurements, except in one case which is highlighted in gray color in Table III, are higher than those of the repeated measurements.

Figs. 8 and 9 depict the Empirical Cumulative Distribution Functions (ECDFs) of the means ($\mu_{_{Sync}}$ vs. $\mu_{_{Rep}}$) and the standard deviations ($\sigma_{_{Sync}}$ vs. $\sigma_{_{Rep}}$) for the different LSPs and they confirm the aforementioned two findings.

4) *Detailed Investigation of a Specific Case*

In the sequel we investigate an extreme case where the estimates of the cross-correlation coefficient of the delay spread (ρ_{σ_τ}) from the synchronous measurements have 10 times the standard deviation of the estimates from the repeated measurements, where $\mu_{\sigma_\tau,Sync} \approx \mu_{\sigma_\tau,Rep}$, and $\sigma_{\sigma_\tau,Sync} > 10\sigma_{\sigma_\tau,Rep}$. See the cells with bold values in Tables II and III. When synchronous measurements are used, cross-correlation coefficients of 0.43, 0.37 and 0.17 are estimated using run 1, run 2 and run 3, respectively. However, estimating the cross-correlation coefficient from repeated measurements gives approximately 0.35 regardless of the used measurement runs. The investigated time series pairs are depicted in Fig. 10 along with their associated cross-correlation coefficients. A quick look at these plots is not enough to explain the reason behind the higher spread among the 3 estimates from synchronous measurements compared to the low spread of the 3 estimates from repeated measurements. Therefore, let's take a closer look at the time series of subplots (a), (c), and (e) of Fig. 10 (total of 6 time series), which correspond to performing the estimation based on: synchronous measurements using run 1 ($\rho_{\sigma_\tau,EM,Sync,R1} = 0.43$), synchronous measurements using run 3 ($\rho_{\sigma_\tau,EM,Sync,R3} = 0.17$), and repeated measurements using runs 1 & 3 ($\rho_{\sigma_\tau,EM,Rep,R1\&R3} = 0.34$), respectively. In Fig. 11, for each of these 3 cases, we plot: 1) the corresponding zero-mean unit-variance time series, and 2) C_{σ_τ}, which is defined as the time series resulting from the element-wise multiplication of the corresponding pair of the zero-mean unit-variance time series (please see the definitions of (2)). C_{σ_τ} allows us to identify the contribution of each segment of snapshots (i.e.,

TABLE I
MEASUREMENT RUNS USED FOR THE TWO APPROACHES: SYNCHRONOUS VERSUS REPEATED MEASUREMENTS

	1st estimate	2nd estimate	3rd estimate
Synchronous	Run 1	Run 2	Run 3
Repeated	Run 1 & 2	Run 1 & 3	Run 2 & 3

TABLE II
THE VALUES OF THE MEAN OF THE CROSS-CORRELATION ESTIMATES (μ) USING THE SYNCHRONOUS VERSUS THE REPEATED MEASUREMENT APPROACHES

	ES	EF	EM	SF	SM	FM
$\mu_{LSF,Sync}$	0.16	~~0.12~~	0.80	0.25	~~-0.12~~	-0.18
95% CI	[0.02, 0.29]	[-0.01, 0.25]	[0.74, 0.84]	[0.11, 0.37]	[-0.25, 0.01]	[-0.30, -0.04]
$\mu_{LSF,Rep}$	~~0.09~~	~~0.02~~	0.84	0.26	~~-0.10~~	-0.15
95% CI	[-0.04, 0.22]	[-0.11, 0.15]	[0.79, 0.87]	[0.12, 0.38]	[-0.23, 0.03]	[-0.28, -0.01]
$\mu_{\sigma_\tau,Sync}$	0.44	0.30	**0.33**	0.44	-0.47	-0.45
95% CI	[0.32, 0.54]	[0.16, 0.42]	[0.20, 0.44]	[0.32, 0.54]	[-0.57, -0.35]	[-0.55, -0.33]
$\mu_{\sigma_\tau,Rep}$	0.40	0.21	**0.36**	0.46	-0.49	-0.44
95% CI	[0.27, 0.50]	[0.07, 0.33]	[0.23, 0.47]	[0.34, 0.56]	[-0.58, -0.37]	[-0.54, -0.32]
$\mu_{\sigma_\phi,Sync}$	0.37	0.18	0.31	-0.22	-0.17	~~0.07~~
95% CI	[0.24, 0.48]	[0.04, 0.30]	[0.18, 0.42]	[-0.34, -0.08]	[-0.30, -0.03]	[-0.06, 0.20]
$\mu_{\sigma_\phi,Rep}$	0.34	0.14	0.36	-0.20	-0.16	~~0.09~~
95% CI	[0.21, 0.45]	[0.00, 0.27]	[0.23, 0.47]	[-0.32, -0.06]	[-0.29, -0.02]	[-0.04, 0.22]
$\mu_{\sigma_\theta,Sync}$	~~0.12~~	0.35	0.67	~~-0.09~~	~~-0.06~~	~~0.10~~
95% CI	[-0.01, 0.25]	[0.22, 0.46]	[0.58, 0.73]	[-0.21, 0.05]	[-0.19, 0.07]	[-0.03, 0.23]
$\mu_{\sigma_\theta,Rep}$	~~0.13~~	0.39	0.68	~~-0.01~~	~~-0.04~~	~~0.09~~
95% CI	[0.00, 0.26]	[0.26, 0.50]	[0.59, 0.74]	[-0.14, 0.12]	[-0.17, 0.09]	[-0.04, 0.22]

TABLE III
THE VALUES OF THE STANDARD DEVIATION OF THE CROSS-CORRELATION ESTIMATES (σ) USING THE SYNCHRONOUS VERSUS THE REPEATED MEASUREMENT APPROACHES

	ES	EF	EM	SF	SM	FM
$\sigma_{LSF,Sync}$	0.078	~~0.089~~	0.086	0.036	~~0.017~~	0.068
$\sigma_{LSF,Rep}$	~~0.005~~	~~0.078~~	0.032	0.026	~~0.024~~	0.034
$\sigma_{\sigma_\tau,Sync}$	0.107	0.072	**0.138**	0.010	0.026	0.114
$\sigma_{\sigma_\tau,Rep}$	0.056	0.071	**0.012**	0.009	0.006	0.050
$\sigma_{\sigma_\phi,Sync}$	0.049	0.098	0.094	0.020	0.022	~~0.088~~
$\sigma_{\sigma_\phi,Rep}$	0.014	0.060	0.016	0.009	0.015	~~0.010~~
$\sigma_{\sigma_\theta,Sync}$	~~0.026~~	0.163	0.025	~~0.131~~	~~0.053~~	~~0.090~~
$\sigma_{\sigma_\theta,Rep}$	~~0.019~~	0.093	0.014	~~0.020~~	~~0.041~~	~~0.057~~

[1] After rounding the values of $\mu_{_{Sync}}$ and $\mu_{_{Rep}}$ to two decimal places, both approaches: 1) directly averaging the cross-correlation estimates, ρ_k, and 2) averaging their corresponding z values then apply the inverse Fisher's transformation, give the same results that are reported in Table II.

This is the author's version of an article that has been published in this journal. Changes were made to this version by the publisher prior to publication.
The final version of record is available at http://dx.doi.org/10.1109/TVT.2017.2691474

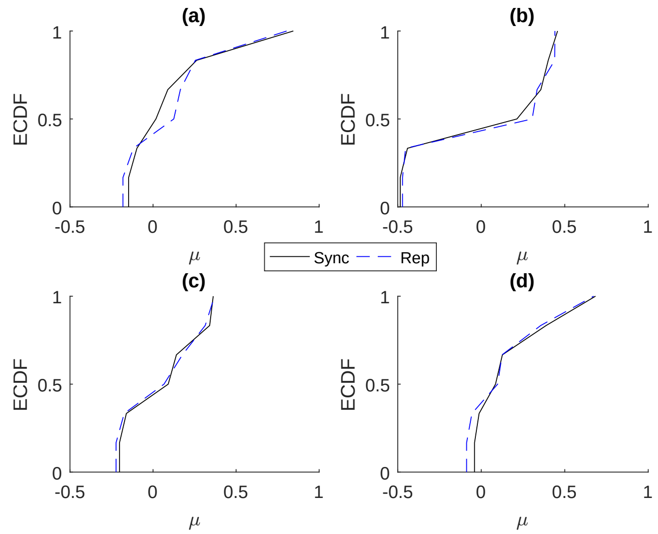

Fig. 8. ECDFs of the values of the mean (μ) of the cross-correlation coefficient for the four LSPs collected from all considered link pairs. (a) the LSF, (b) the delay spread, (c) the azimuth spread, and (d) the elevation spread.

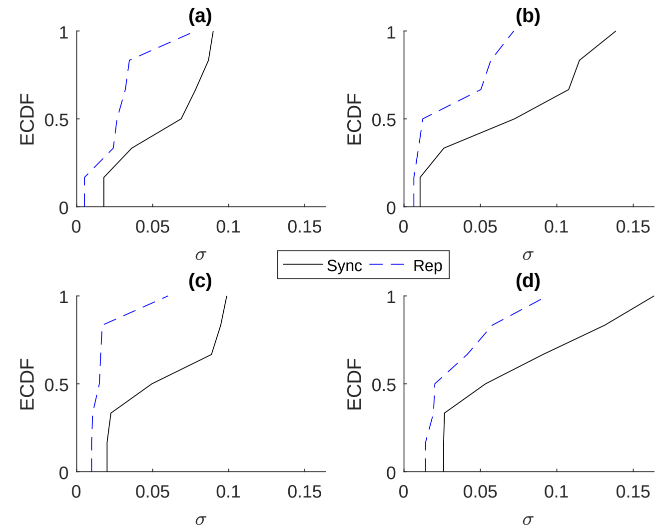

Fig. 9. ECDFs of the values of the standard deviation (σ) of the cross-correlation coefficient for the four LSPs collected from all considered link pairs. (a) the LSF, (b) the delay spread, (c) the azimuth spread, and (d) the elevation spread.

the location of the Rx) towards the value of the estimated cross-correlation coefficient. Fig 11. (a), (c), and (e) depicts the zero-mean unit-variance time series of the delay spread (σ_τ) of links E and M used to estimate: $\rho_{\sigma\tau,EM,Sync,R1}$ from run 1 of the synchronous measurement, $\rho_{\sigma\tau,EM,Sync,R3}$ from run 3 of the synchronous measurement, and $\rho_{\sigma\tau,EM,Rep,R1\&R3}$ from run 1 & run 3 of the repeated measurements, respectively. It is found that:

- The relative high value of $\rho_{\sigma_\tau} = 0.43$ captured by the synchronous measurements in run 1 (time series corresponding to Fig. 11(a)) is driven by the *sudden* high positive contributions of C_{σ_τ} at the first 10 segments (i.e., the first 6 m) of the route as seen in Fig. 11(b). These positive contributions are reduced to almost half during run 3: see the time series of Fig. 11(c) and their corresponding C_{σ_τ} in Fig. 11(d).
- Due to combining time series form run 1 and run 3, the repeated measurements captures a moderate positive contribution from these 10 segments (less than those of the synchronous measurement of run 1, and more than those of the synchronous measurement of run 3). See the time series of Fig. 11(e) and their corresponding C_{σ_τ} in Fig. 11(f).
- The low value of $\rho_{\sigma_\tau} = 0.17$ captured by synchronous measurements in run 3 is driven by the negative contributions of C_{σ_τ} at segments 15 to 21 (i.e., travel distance 9 to 12 m) and the last 15 segments (9 m) of the route, see the time series of Fig. 11(c) and their corresponding C_{σ_τ} in Fig. 11(d). These negative contributions are reduced significantly during run 1, Fig. 11(b), and also not captured by the repeated measurements, Fig. 11(f).

Based on the aforementioned observations, we conclude that the large spread in the estimates of the synchronous measurements is due to *sudden* small changes in the propagation environment (e.g., moving of tree branches). These small changes in the environment are captured by the synchronous measurements; hence, the cross-correlation values

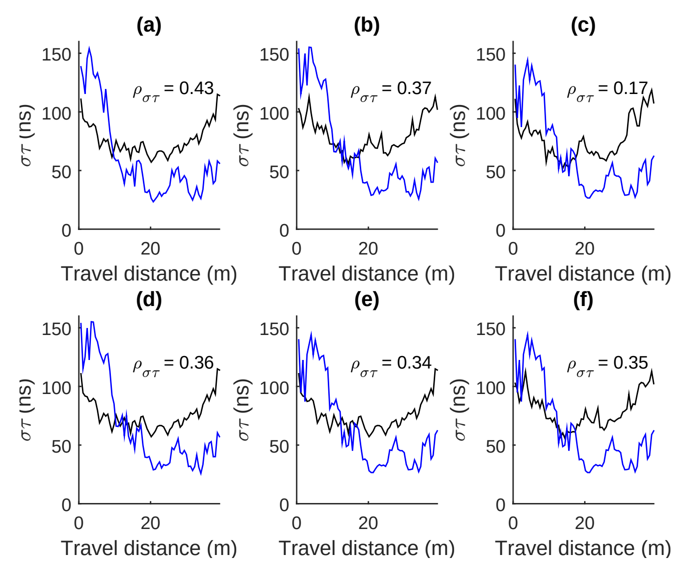

Fig. 10. Examples of the time series estimates of the delay spread (σ_τ) from the three measurement runs, for the E (black) and the M (blue) links, and the corresponding estimated cross-correlation coefficient using synchronous and repeated measurements. Synchronous measurements: (a), (b) and (c), where run 1, run 2, and run 3 are used, respectively. Repeated measurements: (d), (e), and (f), where Runs 1 & 2, Runs 1 & 3, and Runs 2 & 3 are used, respectively.

exhibit higher spread from a measurement run to another. However, due to the randomness of these changes, their effect is ***averaged out*** when the instances of the LSPs of the considered links are measured in two different runs (i.e., repeated measurements). The aforementioned findings are based on limited measurement data set - a total of 24 (4 LSPs $\times$ 6 link pairs) cases each of which has 3 cross-correlation coefficient estimates. Therefore, in the next section, we use Monte Carlo simulations in order to validate these findings.

This is the author's version of an article that has been published in this journal. Changes were made to this version by the publisher prior to publication.
The final version of record is available at http://dx.doi.org/10.1109/TVT.2017.2691474

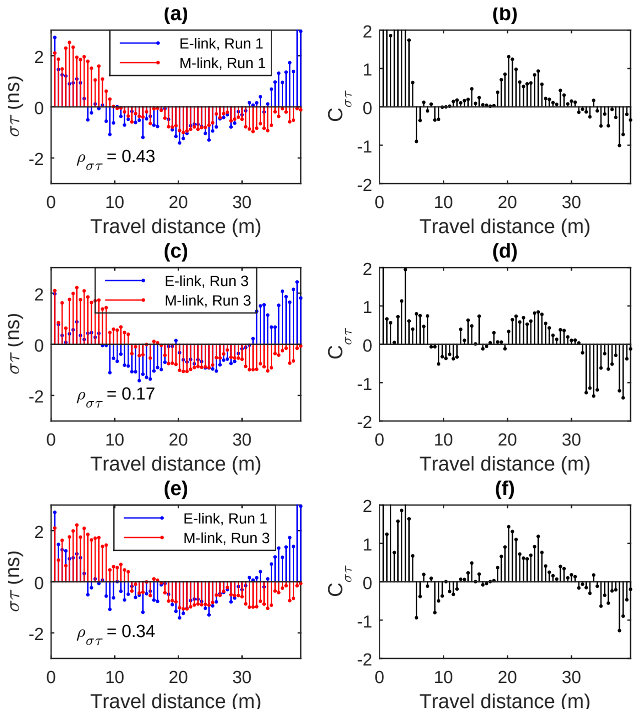

Fig. 11. (a) Zero-mean unit-variance time series counterparts of Fig. 10.a, i.e., synchronous measurements run 1, (c) Zero-mean unit-variance time series counterparts of Fig. 10.c, i.e., synchronous measurements run 3, and (e) Zero-mean unit-variance time series counterparts of Fig. 10.e, i.e., repeated measurements using run 1 & run 3 . (b), (d), and (f) are the element-wise product of the corresponding zero-mean unit-variance time series (C_{σ_τ}). Note that, to simplify the visual comparison, the limits of the y-axis for the plots in (b), (d), and (f) are set to +/- 2.

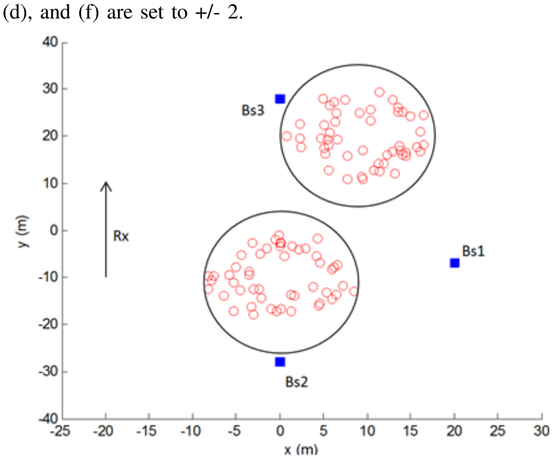

Fig. 12. Schematic diagram of a simulation trial. Small red circles are the 100 scattering points distributed in 2 clusters. The locations of the clusters are indicated by the black circles. Bs1, Bs2, and Bs3 are the 3 base stations and their locations are indicated by the blue squares. The arrow indicates the trajectory of the Rx movement.

B. Simulation Study

We assume a simulation area with three BSs and one Rx which is traveling over a 20 m route. Each simulation run consists of 200 time instances, which corresponds to the traveling time of the Rx through the route. We assume 100 scattering points distributed randomly in two clusters as shown in Fig. 12. These scattering points represent collections of small objects that can be subject to random movement, for example, branches of trees. We assume each scattering point to move according to a random walk model with a 5 cm step size (one step per simulation time instance). The movement

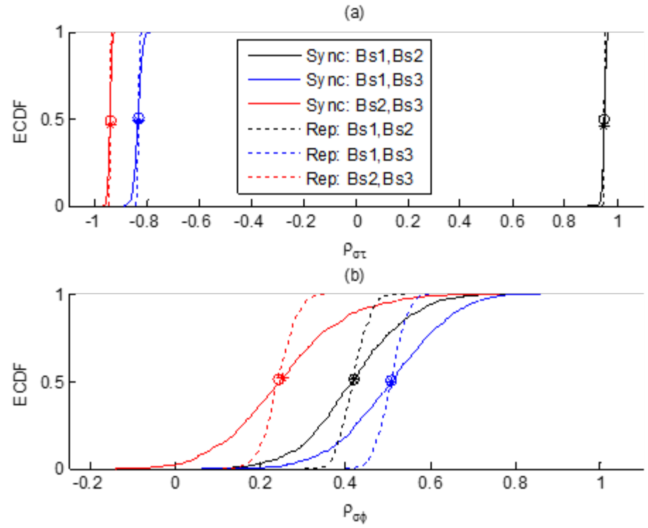

Fig. 13. ECDFs of the estimates of the cross-correlation coefficients using the synchronous and the repeated approaches based on 1000 simulation trials. (a) Cross-correlation of the delay spread (ρ_{σ_τ}), and (b) Cross-correlation of the azimuth spread (ρ_{σ_ϕ}). The stars and circles signify the mean of each ECDF.

of each scattering point is contained within a 1 meter radius circle centered at its origin. Also, during each simulation run, sudden changes in the environment might occur. When a sudden change occurs, new distributions of the scattering points within their clusters take place. At each time instance, we calculate the delay and azimuth spread of each link, where a simple path loss model with $n = 3$ is applied and the loss at each scattering point is ignored. The power variation of each cluster throughout the Rx route follow the model introduced in [23] with slope = 1 dB/m.

The cross-correlation of the delay spread and the azimuth spread of the three link pairs is estimated based on the assumption of having: 1) synchronous measurements and 2) repeated measurements. 1000 simulation trials are performed during which the locations of the clusters, BSs, and the route of the Rx do not change. The differences among the simulation trials are: the distribution of the scattering points within the 2 clusters, and the instances at which abrupt changes occur, where we assume sudden changes to occur according to a Poisson random process with an average of 4 sudden changes during the Rx travel time. The ECDFs of the 1000 estimates of each cross-correlation coefficient for each case (i.e., synchronous measurements and repeated measurements) are depicted in Fig. 13 and they clearly demonstrate the main findings of this work: 1) the repeated measurements are able to capture the mean value of the cross-correlation coefficients and, 2) the cross-correlation estimates from the repeated measurements have less spread around the mean than those resulting from the synchronous measurements.

V. Conclusion

Multi-link propagation measurements were performed with four BSs and one mobile station to compare the accuracy of estimating the properties of the cross-correlation of different large-scale parameters using repeated measurements versus using synchronous measurements. The considered environment is semi-static i.e., the large interacting objects are strictly stationary and there is no significant movement of any interacting object except sudden small movements of tree branches due to wind. Based on the measurements and confirmed by Monte Carlo simulations, it is found that: 1) The means of the cross-correlation coefficients estimated using the two approaches are similar. 2) The cross-correlation estimates from synchronous measurements captures the effect of the abrupt changes in the environments (movements of tree branches due to wind); thus, they exhibit high spread. 3) The cross-correlation coefficient estimates from repeated measurements exhibit lower spread because the effects of the abrupt changes in the environments are averaged out when the instances of the large-scale parameters are measured in different runs.

REFERENCES

[1] N. Czink, B. Bandemer, G. Vazquez-Vilar, L. Jalloul, C. Oestges, and A. Paulraj, "Spatial separation of multi-user MIMO channels," in *IEEE 20th International Symposium on Personal, Indoor and Mobile Radio Communications*, (Toyko, Japan), pp. 1059–1063, Sep. 2009.

[2] C. Oestges, P. Castiglione, and N. Czink, "Empirical modeling of nomadic peer-to-peer networks in office environment," in *IEEE 73rd Vehicular Technology Conference (VTC Spring)*, (Budapest, Hungary), pp. 1–5, May 2011.

[3] V. M. Kolmonen, P. Almers, J. Salmi, J. Koivunen, K. Haneda, A. Richter, F. Tufvesson, A. F. Molisch, and P. Vainikainen, "A dynamic dual-link wideband MIMO channel sounder for 5.3 GHz," *IEEE Transactions on Instrumentation and Measurement*, vol. 59, pp. 873–883, Apr. 2010.

[4] J. Poutanen, K. Haneda, V. M. Kolmonen, J. Salmi, and P. Vainikainen, "Analysis of correlated shadow fading in dual-link indoor radio wave propagation," *IEEE Antennas and Wireless Propagation Letters*, vol. 8, pp. 1190–1193, Oct. 2009.

[5] Z. Meifang, F. Tufvesson, and J. Medbo, "Correlation properties of large scale parameters from 2.66 GHz multi-site macro cell measurements," in *IEEE 73rd Vehicular Technology Conference (VTC Spring)*, (Budapest, Hungary), pp. 1–5, May 2011.

[6] B. Lau, M. Jensen, J. Medbo, and J. Furuskog, "Single and multi-user cooperative MIMO in a measured urban macrocellular environment," *IEEE Transactions on Antennas and Propagation*, vol. 60, pp. 624–632, Feb. 2012.

[7] G. Dahman, J. Flordelis, and F. Tufvesson, "On the cross-correlation properties of large-scale fading in distributed antenna systems," in *IEEE Wireless Communications and Networking Conference (WCNC)*, (Istanbul, Turkey), Apr. 2014.

[8] J. Flordelis, G. Dahman, and F. Tufvesson, "Measurements of large-scale parameters of a distributed MIMO antenna system in a microcell environment at 2.6 GHz," in *the 7th European Conference on Antennas and Propagation (EuCAP)*, (Gothenburg, Sweden), pp. 3026–3030, Apr. 2013.

[9] V. Jungnickel, S. Jaeckel, L. Thiele, L. Jiang, U. Kruger, A. Brylka, and C. Von Helmolt, "Capacity measurements in a cooperative MIMO network," *IEEE Transactions on Vehicular Technology*, vol. 58, pp. 2392–2405, June 2009.

[10] S. Jaeckel, L. Thiele, A. Brylka, L. Jiang, V. Jungnickel, C. Jandura, and J. Heft, "Intercell interference measured in urban areas," in *IEEE International Conference on Communications (ICC)*, (Dresden, Germany), pp. 1–6, June 2009.

[11] S. Jaeckel, L. Jiang, V. Jungnickel, L. Thiele, C. Jandura, G. Sommerkorn, and C. Schneider, "Correlation properties of large and small-scale parameters from multicell channel measurements," in *the 3rd European Conference on Antennas and Propagation (EuCAP)*, (Berlin, Germany), pp. 3406–3410, Mar. 2009.

[12] G. S. Dahman, R. J. C. Bultitude, and R. H. M. Hafez, "The use of frequency-orthogonal pseudonoise (FOPN) sounding signals for identifying transmissions from different transmit antennas," *IEEE Antennas and Wireless Propagation Letters*, vol. 8, pp. 657–660, Apr. 2009.

[13] G. Levin, R. J. Bultitude, and H. Zhu, "Modelling, measurement and analysis of narrowband fast fading on relay channels," in *IEEE 22nd International Symposium on Personal Indoor and Mobile Radio Communications (PIMRC)*, (Toronto, Canada), pp. 2065–2069, Sep. 2011.

[14] M. Narandzic, M. Kaske, G. Sommerkorn, S. Jackel, C. Schneider, and R. S. Thoma, "Variation of estimated large-scale MIMO channel properties between repeated measurements," in *IEEE 73rd Vehicular Technology Conference (VTC Spring)*, (Budapest, Hungary), pp. 1–5, May 2011.

[15] R. Thoma, D. Hampicke, A. Richter, G. Sommerkorn, A. Schneider, U. Trautwein, and W. Wirnitzer, "Identification of time-variant directional mobile radio channels," *IEEE Transactions on Instrumentation and Measurement*, vol. 49, pp. 357–364, Apr. 2000.

[16] E. Sousa, V. Jovanovic, and C. Daigneault, "Delay spread measurements for the digital cellular channel in Toronto," *IEEE Transactions on Vehicular Technology*, vol. 43, pp. 837–847, Nov. 1994.

[17] B. Fleury, M. Tschudin, R. Heddergott, D. Dahlhaus, and K. Ingeman Pedersen, "Channel parameter estimation in mobile radio environments using the SAGE algorithm," *IEEE Journal on Selected Areas in Communications*, vol. 17, pp. 434–450, Mar. 1999.

[18] B. Fleury, Y. Xuefeng, K. Rohbrandt, P. Jourdan, and A. Stucki, "Performance of a high-resolution scheme for joint estimation of delay and bidirection dispersion in the radio channel," in *IEEE 55th Vehicular Technology Conference (VTC Spring)*, (Birmingham, AL, USA), pp. 522–526, May 2002.

[19] A. F. Molisch, *Wireless communications*. California, USA: John Wiley and Sons, 2010.

[20] D. J. Sheskin, *Handbook of parametric and nonparametric statistical procedures*. CRC Press, 2003.

[21] C. L. Harrison and D. A. Kenny, *Statistics for the social and behavioral sciences*. Little, Brown and Company, 1987.

[22] R. A. Alexander, "A note on averaging correlations," *Bulletin of the Psychonomic Society*, vol. 28, no. 4, pp. 335–336, 1990.

[23] X. Gao, F. Tufvesson, and O. Edfors, "Massive MIMO channels - measurements and models," in *the 47th Asilomar Conference on Signals, Systems and Computers*, (Pacific Grove, California), pp. 280–284, Nov. 2013.

Ghassan Dahman received his Ph.D. in 2010 from Carleton University, Ottawa, Canada. Between 2010 and 2012, he worked as an assistant professor at Umm Al-Qura University, Makkah, KSA. From 2012 to 2016, he worked as a postdoctoral researcher with Lund University, Lund, Sweden. He is currently working as a researcher at the NSERC-Ultra Electronics TCS Industrial Chair, École de Technologie Suprieure (ÉTS), Montreal, Canada. His main research interests are radio propagation and channel modelling including: massive MIMO, distributed antenna systems, overwater point-to-point communications, and anomalous propagation of microwaves in the troposphere.

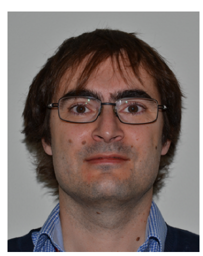

Jose Flordelis received his M.S. degrees in telecommunication engineering from Universitat Politècnica de València, Spain, and from Högskolan i Gävle, Sweden, in 2002. He is currently working toward the Ph.D. degree at the Department of Electrical and Information Technology of Lund University, Sweden. From 2002 to 2012 he was with Ericsson in Sweden, where he contributed to the development of 3GPP LTE- and Bluetooth-based solutions. His main research interests are measurement, characterization, and modelling of wireless channels, especially in the areas of Massive MIMO, and distributed antenna systems.

Fredrik Tufvesson received his Ph.D. in 2000 from Lund University in Sweden. After two years at a startup company, he joined the department of Electrical and Information Technology at Lund University, where he is now professor of radio systems. His main research interests are channel modelling, measurements and characterization for wireless communication, with applications in various areas such as massive MIMO, UWB, mm wave communication, distributed antenna systems, radio based positioning and vehicular communication. Fredrik has authored around 60 journal papers and 120 conference papers, recently he got the Neal Shepherd Memorial Award for the best propagation paper in IEEE Transactions on Vehicular Technology.